2016

Coupled Thermodynamic And CFD Approaches Applied To A Supersonic Air Ejector

Sergio Croquer
Université de Sherbrooke, Canada, sergio.croquer@usherbrooke.ca

Sébastien Poncet
Université de Sherbrooke, Canada, sebastien.poncet@usherbrooke.ca

Nicolas Galanis
Université de Sherbrooke, Canada, nicolas.galanis@usherbrooke.ca

Coupled Thermodynamic and CFD Approaches Applied to A Supersonic Air Ejector

Sergio CROQUER[1]*, Sébastien PONCET[2], Nicolas GALANIS[3]

[1]Université de Sherbrooke, Département de Génie Mécanique,
Sherbrooke, Quebec, Canada
Contact Information (Sergio.Croquer@USherbrooke.ca)

[2]Université de Sherbrooke, Département de Génie Mécanique,
Sherbrooke, Quebec, Canada
Contact Information (Sébastien.Poncet@USherbrooke.ca)

[3]Université de Sherbrooke, Département de Génie Mécanique,
Sherbrooke, Quebec, Canada
Contact Information (Nicolas.Galanis@USherbrooke.ca)

* Corresponding Author

ABSTRACT

This paper presents a systematic comparison of ejector performance predictions between a thermodynamic model and a Computational Fluid Dynamics (CFD) model for different operating conditions. The thermodynamic model developed by Galanis and Sorin (2016) assumes the primary flow is always choked, and irreversibilities due to viscous dissipation are taken into account through polytropic efficiencies. The CFD model developed by Croquer *et al.,* (2016a) on a commercial software has already been validated for supersonic ejectors working with R134a, taking a standard high Reynolds number k-ω SST turbulence model coupled with the perfect gas law.
The dimensions of the ejector were first determined by the thermodynamic model and then used in the CFD model. The thermodynamic model predicts higher entrainment ratios for double choking operation and somewhat different values of the critical and limiting pressure ratios. The CFD model validates the similarity solutions characteristic of ejectors using perfect gases. The present results show in particular that identical inlet pressure and temperature ratios induce the same entrainment ratio as well as the same critical and limiting pressure ratios. Both models confirm also that similar diameter ratios between the primary nozzle throat and the constant area section lead to the same values of the entrainment ratio. Thus, for double-choking operations, the entrainment ratio depends on the inlet pressure and temperature ratios rather than on the individual values of these four properties as it is the case for ejectors with real fluids. It also shows that the position of the shock varies linearly with the compression ratio in qualitative agreement with the assumption used in the thermodynamic model.

1. INTRODUCTION

Supersonic ejectors are simple devices with applications in a wide range of industries. Particularly, in the cooling sector, ejector expansion refrigeration cycles (EERC) have received special interest in the last decades, due to their better performance over compressor refrigeration cycles, lower maintenance requirements and capacity to use low quality thermal energy as power source (Chunnamond and Aphornratana, 2004a). Other fields in which ejectors are often found are: gas production, steam power plants, and nuclear energy safety systems.

Figure 1 presents a general schematic of the main sections of a supersonic ejector: primary nozzle, secondary inlet, mixing zone, constant area section and outlet diffuser. In a supersonic ejector, a high energy motive flow is accelerated through the primary nozzle, entering the mixing section as a supersonic stream at low pressure which entrains the secondary flow. Due to the high velocity difference, the entrained flow is confined and accelerated between the primary jet and the ejector walls (Huang *et al.,* 1999), and it is slowly accelerated by shear friction until it reaches sonic condition, at which point mixing starts. The supersonic mixture goes through a series of shocks along the constant area section, entering the diffuser as a subsonic flow.

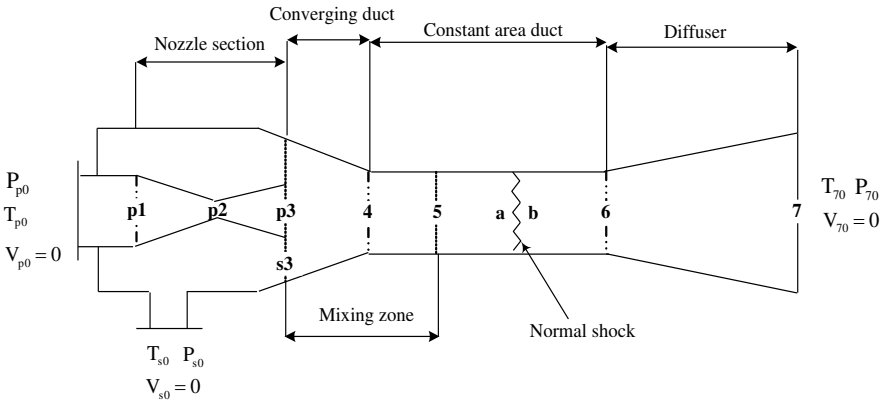

Figure 1: Schematic representation of a typical ejector geometry with relevant notations.

Ejector performance is measured using the entrainment ratio (ω), the proportion of secondary to primary mass flow, and the compression ratio (PR), the ratio of outlet or back pressure to secondary inlet pressure, P_7/ P_{s0}. Figure 2 presents a typical operating curve of a supersonic ejector, i.e.: ω as a function of the outlet pressure (P_7). For back pressure values lower than the critical pressure (P_c), both inlet flows are supersonic and hence the mass flow is independent of the outlet pressure, this is known as double choking condition (Chunnamond and Aphornratana, 2004a). For back pressure values greater than P_c but smaller than the limiting pressure (P_{lim}), the secondary flow is no longer choked and the entrainment ratio drops rapidly. This region is known as single choke operation. Beyond P_{lim}, the ejector malfunctions, i.e., the primary flow deviates toward the secondary inlet, and thus the entrainment ratio becomes negative.

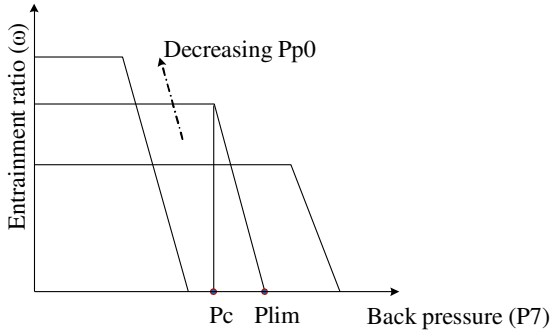

Figure 2: Typical performance curves for an ejector of fixed geometry and constant secondary fluid inlet conditions.

Ejector performance is closely related to its geometry (Milazzo *et al.,* 2014). Huang *et al.,* (1999) found that the optimal area ratio (Ar) for single phase ejectors lies in the range 7-10. Garcia *et al.,* (2014) showed the dependency of ω with the Nozzle Exit Position (NXP) (the distance between sections p3 and 4) in a single phase R134a ejector. In this regard, the main goal of thermodynamic or one-dimensional

models is to obtain the best performing geometry for a given set of operating conditions. They include several assumptions to avoid the calculation of complex phenomena present in real ejectors (such as shock-boundary layer interactions and supersonic shear layers). A pioneering model is the one of Keenan *et al.,* (1950), which is based on the 1D equations for compressible isentropic flows with added assumptions, namely: the shock position is fixed beforehand, the pressure of both inlet fluids is the same at the start of the mixing section, losses are accounted for using isentropic coefficients, and the fluid behaves as a perfect gas. Subsequent models of increased complexity have been published, such as those of Stoecker and Jones (1958), Munday and Bagster (1977), Huang *et al* (1999) and Liu and Groll (2013).
With the recent advances in computing power, the application of Computational Fluid Dynamics models to represent the flow throughout supersonic ejectors has drastically increased. These models, with far greater complexity than the thermodynamic models, offer information on the flow field inside the ejector, comprising quantities which are inaccessible via experiments (Pianthong *et al.,* 2007, Bartosiewicz *et al.,* 2005). This approach solves the governing equations of compressible flows for a fixed ejector geometry and inlet-outlet conditions, without assumptions concerning the shock position, the isentropic behavior or pressure conditions at internal sections of the ejector.
This paper presents a systematic comparison of the results given by the thermodynamic model of Galanis and Sorin (2016) and a CFD model developed on a commercial code and previously validated in Croquer *et al.,* (2016a,b). The thermodynamic model introduces the application of polytropic efficiencies instead of isentropic coefficients. On the other hand, the CFD only keeps the assumptions of perfect gas and axisymmetric behavior.
The dimensions of a single phase ejector, with air as working fluid, were determined using the thermodynamic model for different inlet pressure ratios (P_{p0}/P_{s0}): 60, 100 and 140 and a fixed inlet temperature ratio $T_{p0}/T_{s0} = 1.6$. The thermodynamic model relies on the similarity solutions characteristic of ejectors using perfect gases. This assumption is validated by the CFD model reproducing the operating conditions at different specific values of the inlet secondary pressure (P_{s0} = 50663 Pa, 101325 Pa and 202650 Pa) and primary nozzle throat diameter (D_{p2} = 0.02 m and 0.06 m).

2. MODELING PROCEDURE

The dimensions of the ejector were calculated with the thermodynamic model for a back pressure equal to the limiting critical value (P_c), and using the following input parameters: P_{p0}/P_{s0}= 100, T_{p0}/T_{s0}= 1.6, ω = 0.2 and all polytropic efficiencies equal to 0.9. This was defined as the on-design operating condition. Afterward, the ejector geometry was assessed at P_{p0}/P_{s0} values of 60 and 140. The chosen polytropic efficiency value corresponds to equivalent isentropic and mixing efficiencies within the range 0.7 to 1.0 (Liu and Groll, 2013).
The geometry determined with the thermodynamic model is expressed in terms of non-dimensional diameters and lengths: D_{p1}/D_{p2} = 2.36, D_{p3}/D_{p2} = 3.69, D_3/D_{p2} = 5.43, $D_4/D_{p2} = D_6/D_{p2}$ = 4.96, D_7/D_{p2} = 10.65, x_2/D_{p2} = 3.87, x_3/D_{p2} = 19.28, x_4/D_{p2} = 20.61, x_6/D_{p2} = 96.14, x_7/D_{p2} = 111.10.
Ejector geometrical scalability was assessed by considering two different primary throat sizes: D_{p2} = 0.02 m and 0.06 m. The effect of the secondary inlet pressure value was investigated by considering three P_{s0} values (50663 Pa, 101325 Pa and 202650 Pa) for a fixed ratio P_{p0}/P_{s0}= 100.
In this investigation, the working fluid is air considered as an ideal gas with constant thermophysical properties (R = 287 J/kg/K, γ = 1.4, k = 0.0242 W/m/K, $\mu = 1.7894 \times 10^{-5}$ kg/m/s).

2.1 Thermodynamic Model

The thermodynamic model assumes a perfect gas behavior in a one dimensional flow field. Distinct from the vast majority of ejector 0D and 1D models, this approach introduces polytropic efficiencies to account for losses during the acceleration and diffusion processes (sections p0 to p3, s0 to s3 and 6 to 7 in Figure 1). Primary and secondary flows are accelerated from states p0 and s0 respectively toward section 3, where mixing at constant pressure starts. At position 5, mixing is complete. A normal shock is assumed to

occur at the constant area section, at a location which depends linearly on the outlet to secondary inlet pressure ratio. Thus at the diffuser inlet (position 6), the mixture is always subsonic.
The model takes gas properties (R, γ), total pressure and temperature at inlets, primary nozzle throat area, entrainment ratio and polytropic coefficients as data input. An iterative process on the equations of mass, momentum and energy is followed at the limit of double-choke operation (P_c) to determine the thermodynamic states and ejector dimensions at every distinctive section, for given inlet conditions and entrainment ratio. The model also allows to compute single-choke operation (outlet pressure greater than P_c) for a fixed geometry and inlet conditions.

2.2 CFD (RANS) Model

An axisymmetric, steady-state RANS model was developed using the finite volume package ANSYS Fluent v.15. The ejector geometry resulting from the thermodynamic model was defined as the computational domain. Figure 3 shows the mesh used for spatial discretization, this grid consisted of 67000 elements, achieving an average Y+ value of 76, which is adequate for the chosen turbulence model (k-ω SST in its high-Reynolds number formulation). A grid independence study, taking into account entrainment ratio and Mach number profiles along the ejector centerline, was used to verify result invariability with different spatial discretizations.

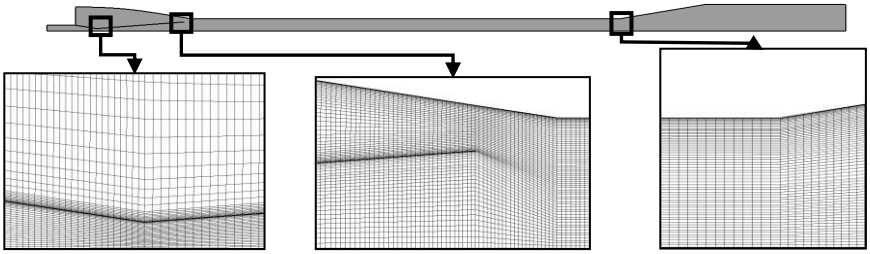

Figure 3: Details of the mesh grid used in the CFD calculations.

Despite its greater differences with experimental results (Cai and He, 2013), the ideal gas model was chosen since it retains the assumptions made in the thermodynamic model. On the other hand, the k-ω SST model in its high-Reynolds number approach was chosen, given its better prediction of the ejector internal flow structure, particularly around the shock region in comparison with the k-ε model (Croquer *et al.,* 2016a).
The conservation equations of mass, momentum, energy and turbulent quantities, together with the ideal gas equation of state, were considered as the flow governing equations. The system of governing equations was solved by a finite volume approach, with a density based solver, which is known to offer better results in systems involving high compressibility effects and sharp variations in flow properties. A 2nd order upwind scheme was used in the spatial discretization of the convective terms of the continuity, momentum and energy equations, while a 1st order upwind was adopted for the turbulent quantities. All the diffusive terms were discretized with a 2nd order central scheme.
The boundary conditions were chosen according to the operating conditions determined by the thermodynamic model. Total pressure and temperature values were prescribed at both inlets, with a turbulent intensity of 5%, whereas static pressure was fixed at the outlet. Walls were considered smooth and adiabatic.

3. RESULTS

3.1 Ejector operating curve

Figure 4 shows a comparison of predicted performance curves for a fixed geometry ejector and three values of P_{p0}/P_{s0} and T_{p0}/T_{s0} = 1.6. The qualitative effect of P_{p0}/P_{s0} on the predictions of the two models is the same, and corresponds with theoretical and experimental observations (Chunnamond and

Aphornratana, 2004a). At double choke conditions, the thermodynamic model predicts a greater entrainment ratio than the CFD model, the difference being 0.055, 0.055 and 0.05 points for inlet pressure ratios (P_{p0}/P_{s0}) of 60, 100 and 140 respectively. This difference suggests a conservative value of the losses coefficient in the thermodynamic model, and reflects the numerous assumptions taken by the latter in comparison with the CFD model. Critical pressure values are practically identical between both models, except for P_{p0}/P_{s0} = 100 where the predicted values are 5.72 and 6.10 for the thermodynamic and CFD models respectively.

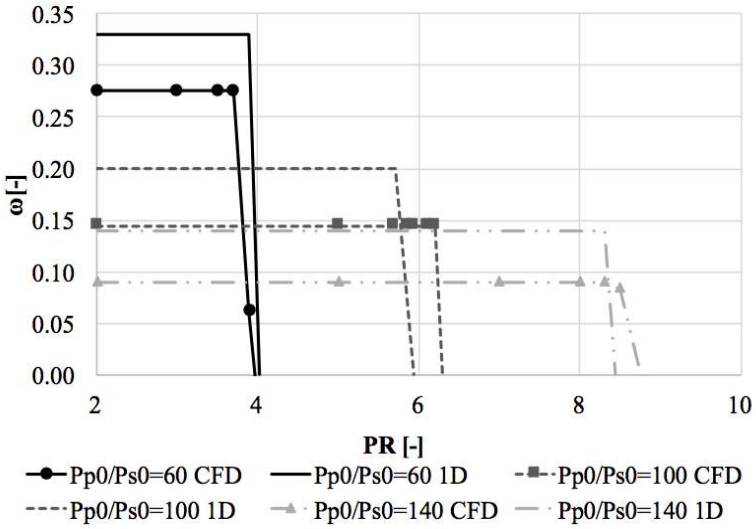

Figure 4: Comparisons between the CFD and thermodynamic models in terms of the ejector entrainment ratio versus the compression ratio (P_7/P_{s0}), for P_{p0}/P_{s0} = 60, 100 and 140. Results obtained for D_{p2}=0.02 m, P_{s0} = 101325 Pa, and T_{p0}/T_{s0} = 1.6 (T_{s0} = 300 K).

3.2 Ejector scalability, effect of Dp2

A comparison of the performance and internal pressure profiles between two geometrically similar ejectors with D_{p2} = 0.02 m and 0.06 m is shown in Figures 5a and 5b respectively, the results were obtained with the CFD model for P_{p0}/P_{s0} = 100 (P_{s0} = 101325 Pa), T_{p0}/T_{s0} = 1.6 (T_{s0} = 300 K). It is observed that under the same operating conditions, geometrically similar ejectors have the same double choke entrainment ratio and critical pressure, with slight differences in the single choke slope and malfunctioning pressure. Regarding the internal flow field, Figure 5b shows that the ejector size affects the shock structure. An increase in D_{p2} leads to a later start of the shock train and a higher pressure jump in comparison with D_{p2} = 0.02 m. Nonetheless, there is virtually no difference in the profiles before the shock nor at the start of the diffuser section, which relates to the identical double choke entrainment ratio shown above.

3.3 Ejector scalability, effect of Ps0

Figures 6a and 6b depict respectively the ejector operating curve and P/P_{s0} profiles at the centerline of the constant area section for different values of P_{s0}: 50663 Pa, 101325 Pa and 202650 Pa, maintaining the inlet conditions ratios P_{p0}/P_{s0} = 100 and T_{p0}/T_{s0} = 1.6 (T_{s0} = 300 K) for the ejector with D_{p2} = 0.02 m. These figures verify that ejector single and double choke performance depend on the ratios P_{p0}/P_{s0} and T_{p0}/T_{s0}, rather than on the specific values of the operating conditions, when the perfect gas law is applied. Since this behavior is observed both in the thermodynamic and CFD models, it must be a result of the nature of the working fluid. The profiles of Figure 6b show that the shock train starting position and intensity is identical among the three values of P_{s0} considered at double choke conditions.

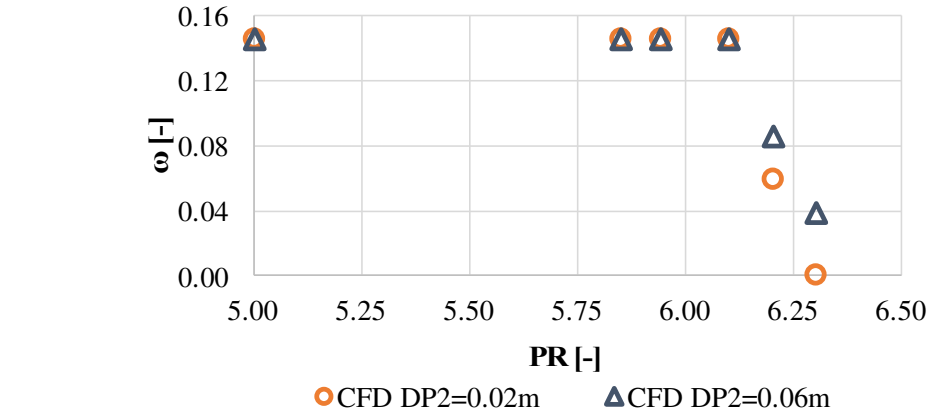

(a)

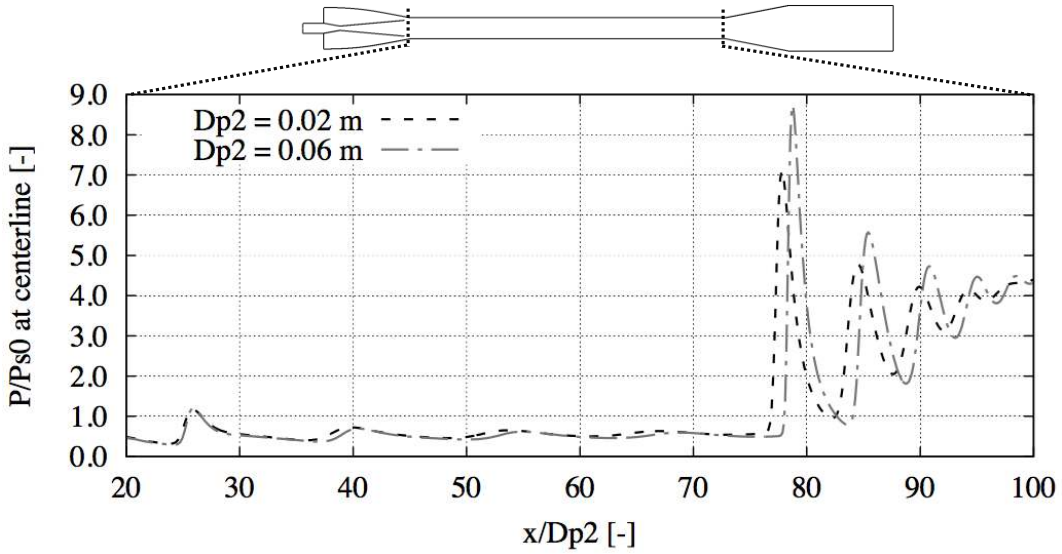

(b)

Figure 5: Ejector entrainment ratio ω versus compression ratio P_7/P_{s0} (a), and P/P_{s0} profiles along its centerline with $P_7/P_{s0} = 5$ (b), for two different ejector sizes ($D_{p2} = 0.02$ m and 0.06 m). Results obtained with the CFD model for $P_{p0}/P_{s0} = 100$ ($P_{s0} = 101325$ Pa) and $T_{p0}/T_{s0} = 1.6$ ($T_{s0} = 300$ K).

3.4 Shock train structure and position

In order to take a closer look at the shock structure along the constant area section, Figure 7 shows profiles of wall P/P_{s0} and centerline Ma number profiles, as well as contours of Ma, along the constant area section of the ejector. Inlet conditions are $P_{p0}/P_{s0} = 100$ ($P_{s0} = 101325$ Pa), $T_{p0}/T_{s0} = 1.6$ ($T_{s0} = 300$K), and ejector size is fixed at $D_{p2} = 0.02$m. The values of PR lie within the double choke range.

A slight difference in shock start position is observed depending on the selected criterion: as a discontinuity in the wall pressure profile, or as the start of large oscillations in the centerline Ma profiles. The Ma contours show this is due to the shock train structure, which elongates in the axial direction. Nonetheless, the difference between both values is constant for increasing P_7/P_{s0}. Moreover, the shock train length, defined as the region between shock start (according to the wall pressure criterion) and the point where the centerline Ma value falls under 1, is also constant for increasing values P_7/P_{s0}. This shock configuration implies that, for low values of the pressure ratio P_7/P_{s0}, a portion of the flow entering the subsonic diffuser might be still supersonic, thus affecting its performance.

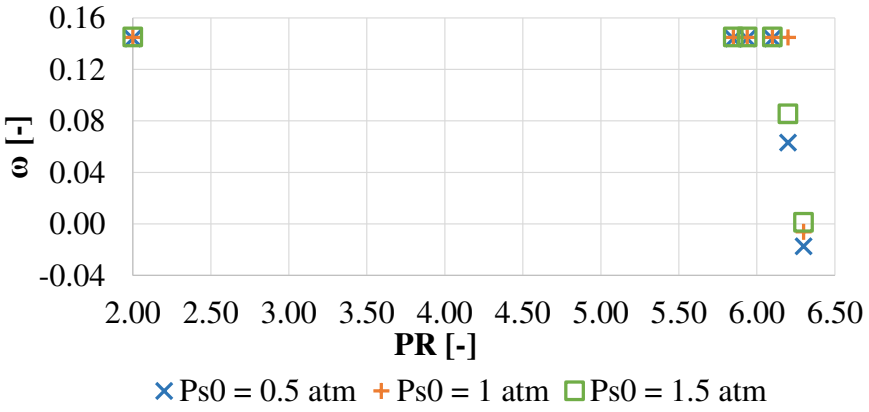

(a)

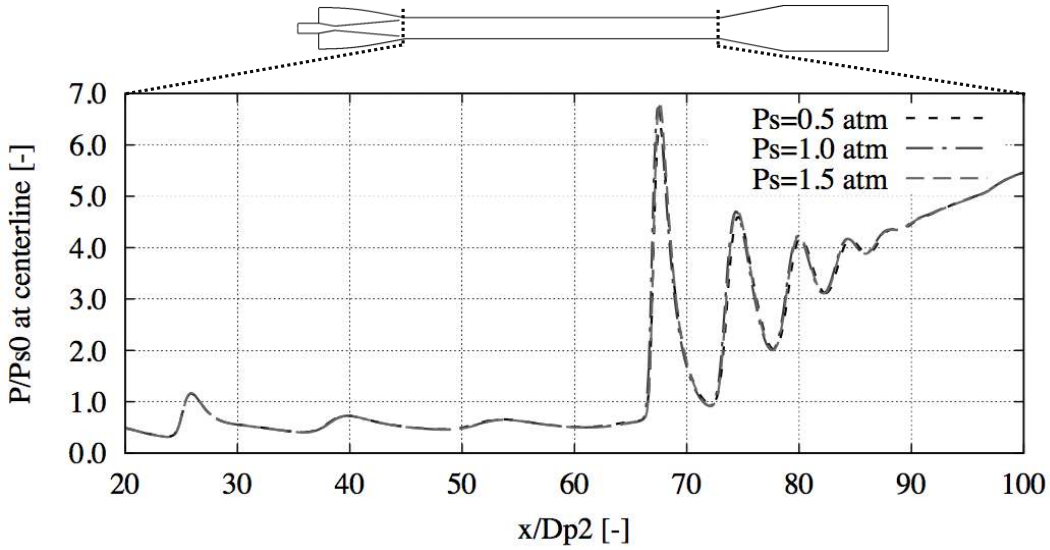

(b)

Figure 6: Ejector entrainment ratio ω versus compression ratio P_7/P_{s0} (a), and P/P_{s0} profiles along its centerline (b), for different P_{s0} values (50663 Pa, 101325 Pa and 202650 Pa). Results obtained with the CFD model for D_{p2}=0.06 m, P_{p0}/P_{s0} = 100 and T_{p0}/T_{s0} = 1.6 (T_{s0} = 300 K).

Figure 8 shows the effect of the compression ratio P_7/P_{s0} over the shock start position (determined using the wall pressure criterion). The shock train starts earlier in the constant area section for increasing P_7/P_{s0} values, which agrees with previous studies (Ruangtrakoon *et al.,* 2013, Croquer *et al.,* 2016b). Moreover, there is a linear relationship between these parameters, which verifies one of the hypothesis of the Thermodynamic model. Nonetheless, the slopes of both models are very different. This reflects that the shock start position range in the CFD model does not covers the whole constant area section within the studied range. Particularly, at on-design conditions, where the Thermodynamic model assumes the shock occurs at x/ D_{p2} = 19, the CFD model shows it starts at a higher value (~ 50).

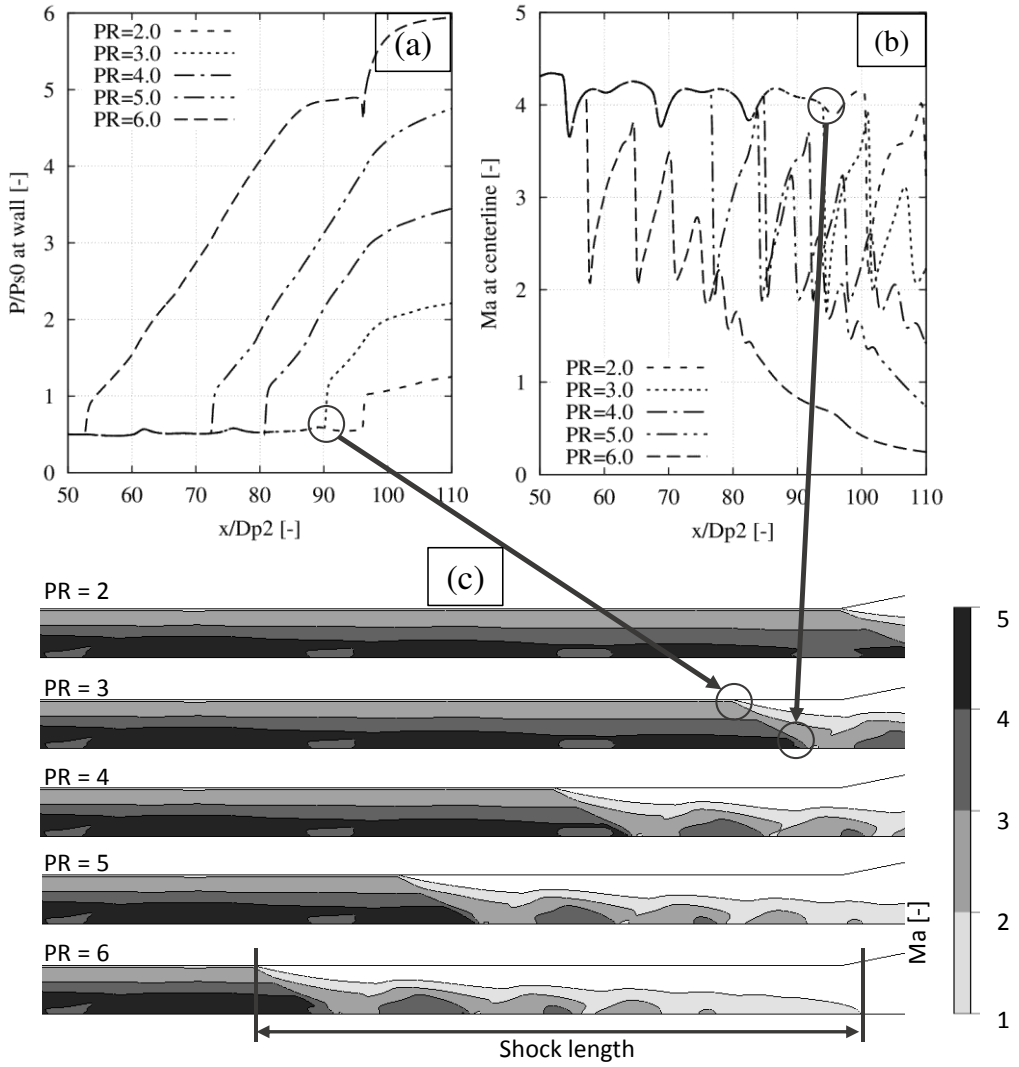

Figure 7: P/P_{s0} profiles at wall (a), Ma number profiles at centerline (b) and Ma contours (c) along the constant area section for increasing PR. Results obtained with the CFD model for $P_{p0}/P_{s0} = 100$ (P_{s0} = 101325 Pa), $T_{p0}/T_{s0} = 1.6$ (T_{s0} = 300 K) and D_{p2} = 0.02 m.

4. CONCLUSIONS

A numerical study of a supersonic ejector with air as perfect gas has been made, comparing the results obtained between the thermodynamic model of Galanis and Sorin (2016), and a 2D axisymmetric model (Croquer *et al.,* 2016a,b). Results show that the thermodynamic model predicts a higher entrainment ratio than the CFD model, in agreement with similar comparisons where the latter better predicts ejector experimental performance (Croquer *et al.,* 2016a). On the other hand, the CFD results show that the scalability of ejector performance in terms of dimensionless ratios (pressure and diameter ratios) is valid when the perfect gas law is applicable. A similar study with real gas properties should be made to verify the range of this assumption to real ejectors. Pressure profiles along the constant area section of the ejector are more sensible to geometrical variations than to specific values of the operating conditions. Thus, an increase in ejector size leads to a shock train of greater intensity, starting further along the

constant area section. On the other hand, an increasing PR leads to earlier starting shock trains, with negligible effect on its structure. The relationship between P_7/P_{s0} and shock start position is linear, although the limiting values do not coincide with the constant area section borders.

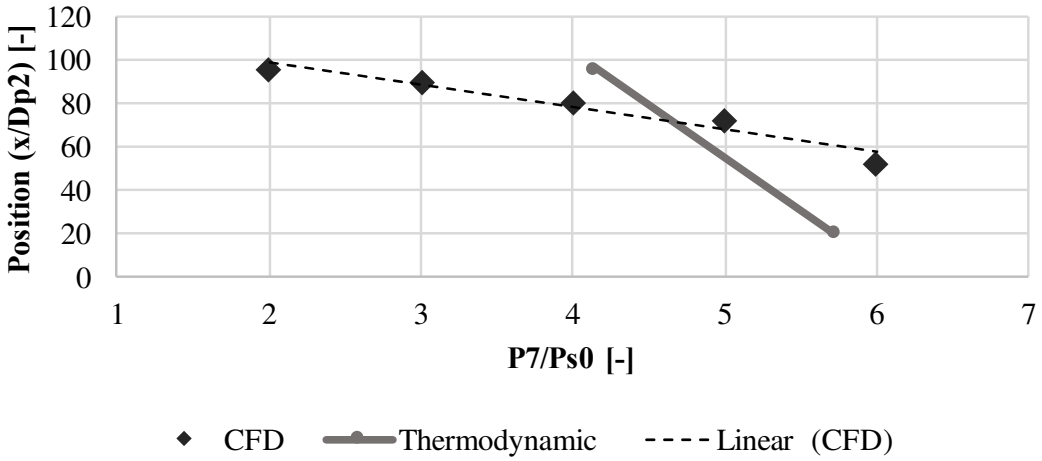

Figure 8: Relationship between shock starting position and PR. Results obtained with the CFD model for P_{p0}/P_{s0} = 100 (P_{s0} = 101325 Pa), T_{p0}/T_{s0} = 1.6 (T_{s0} = 300 K) and D_{p2}= 0.02 m.

NOMENCLATURE

D	Diameter	(m)
K	Thermal conductivity	($W.m^{-1}.K^{-1}$)
$\dot{m}$	Mass flowrate	($kg.s^{-1}$)
Ma	Mach number	(-)
P	Pressure	(Pa)
P_c	Critical pressure	(Pa)
P_{lim}	Limiting malfunction pressure	(Pa)
PR	Compression ratio ($PR = P_{70}/P_{s0}$)	(-)
R	Perfect gas constant	($J.mol^{-1}.K^{-1}$)
T	Temperature	(K)
x	Axial distance from cross-section p1	(m)
Greek letters		
η	Efficiency	(-)
γ	Ratio of specific heats	(-)
μ	Dynamic viscosity	(Pa.s)
ω	Entrainment ratio ($\omega = \dot{m}_s / \dot{m}_p$)	(-)
Subscripts		
0,1,…7	Thermodynamic states at cross sections	
p	Primary	
s	Secondary	

REFERENCES

Bartosiewicz Y., Aidoun Z., Desevaux P. & Mercadier Y. (2005). Numerical and experimental investigation on supersonic ejectors. *International Journal of Heat and Fluid Flow*, 26, 56-70.

Cai L. & He M. (2013). A numerical study on the supersonic steam ejector use in steam turbine system. *Mathematical Problems in Engineering*, 2013, 1-9.

Chunnamond K. & Aphornratana S. (2004a). Ejectors: applications in refrigeration technology. *Renewable & Sustainable Energy Reviews,* 8, 129-155.

Chunnamond K. & Aphornratana S. (2004b). An experimental investigation of a steam ejector refrigerator: the analysis of the pressure profile along the ejector. *Applied Thermal Engineering,* 24, 311-322.

Croquer S., Poncet S. & Aidoun Z. (2016a). Turbulence modeling of a single-phase R134a supersonic ejector. Part 1: Numerical benchmark. *International Journal of Refrigeration,* 61, 140-152.

Croquer S., Poncet S. & Aidoun Z. (2016b). Turbulence modeling of a single-phase R134a supersonic ejector. Part 2: Local flow structure and exergy analysis. *International Journal of Refrigeration,* 61, 153-165.

Galanis N. & Sorin M. (2016). Ejector design and performance prediction. *International Journal of Thermal Sciences*, 104, 315-329

Garcia del Valle J., Saiz Jabardo J.M., Castro Ruiz F. & San Jose Alonso J.F. (2014). An experimental investigation of a R-134a ejector refrigeration system. *International Journal of Refrigeration,* 46, 105-113.

Huang B.J., Chang J. M., Wang C. P. & Petrenko V. A. (1999). A 1-D analysis of ejector performance. *International Journal of Refrigeration,* 22, 354-364.

Keenan J. H., Neumann E. P. & Lustwerk F. (1950). An investigation of ejector design by analysis and experiment. *ASME Journal of Applied Mechanics*, 17, 299-309.

Liu F. & Groll E.A. (2013). Study of ejector efficiencies in refrigeration cycles. *Applied Thermal Engineering,* 52, 360-370.

Milazzo, A., Rocchetti, A. & Eames, I. (2014). Theoretical and Experimental Activity on Ejector Refrigeration. *Energy Procedia,* 45, 1245–1254.

Munday J. T. & Bagster D. F. (1977). A new theory applied to steam jet refrigeration. *Industrial & Engineering Chemical Process Design & Development,* 16 (4), 442-449.

Pianthong K., Seehanam W., Behnia M., Sriveerakul T. & Aphornratana S. (2007). Investigation and improvement of ejector refrigeration system using computational fluid dynamics technique. *Energy Conversion and Management,* 48, 2556–2564.

Ruangtrakoon N., Thongtip T., Aphornratana S. & Sriveerakul T. (2013). CFD simulation on the effect of primary nozzle geometries for a steam ejector in refrigeration cycle. *International Journal of Thermal Sciences,* 63, 133-145.

Stoecker W.F. & Jones J.W. (1958). Refrigeration and Air Conditioning, McGraw Hill, Series in Mechanical Engineering, London.

ACKNOWLEDGEMENTS

This project is part of the research program of the NSERC Chair in Industrial Energy Efficiency, established at Université de Sherbrooke in 2014, with the support of Hydro-Québec, CanmetÉNERGIE, Rio Tinto Alcan and the Natural Sciences and Engineering Research Council of Canada.